# Molecular Dynamics Simulation and Experimental Studies of Gold Nanoparticle Templated HDL-like Nanoparticles for Cholesterol Metabolism Therapeutics

*Cheng-Tsung Lai,[†] Wangqiang Sun,[‡,§,||] Rohun U. Palekar,[‡, §,||] C. Shad Thaxton,[‡, §,||] and George C. Schatz[*,†]*

†Department of Chemistry, Northwestern University, Evanston, Illinois 60208, United States

‡Department of Urology, Northwestern University, Chicago, IL 60611, United States

§Simpson Querrey Institute for Bionanotechnology, 303 E. Superior, Chicago, IL 60611, United States

||International Institute for Nanotechnology, 2145 Sheridan Road, Evanston, IL 60208, United States

KEYWORDS: Apolipoprotein A-I, HDL, gold nanoparticle, cholesterol, cholesteryl ester, LCAT

ABSTRACT

High-density lipoprotein (HDL) plays an important role in the transport and metabolism of cholesterol. Mimics of HDL are being explored as potentially powerful therapeutic agents for removing excess cholesterol from arterial plaques. Gold nanoparticles (AuNPs) functionalized with apolipoprotein A-I, and with the lipids 1,2-dipalmitoyl-sn-glycero-3-phosphocholine and 1,2-dipalmitoyl-sn-glycero-3-phosphoethanolamine-N-[3-(2-pyridyldithio)propionate] have been demonstrated to be robust acceptors of cellular cholesterol. However, detailed structural information about this functionalized HDL AuNP is still lacking. In this study, we have used XPS and LCAT activation experiments together with coarse-grained and all-atom molecular dynamics simulations to model the structure and cholesterol update properties of the HDL AuNP construct. By simulating different apolipoprotein-loaded AuNPs, we find that lipids are oriented differently in regions with and without apoA-I outside the lipid layer. We also show that in this functionalized HDL AuNP, the distribution of cholesteryl ester maintains a reverse concentration gradient that is similar to the gradient found in native HDL.

## INTRODUCTION

High-density lipoprotein (HDL) is involved in the transport and metabolism of phospholipids, triglycerides, and cholesterol. A mature HDL has a size ranging from 7 to 13 nm in diameter and is typically composed of cholesteryl ester, triglycerides, phospholipids, and apolipoproteins. HDL is also known as the carrier of “good” cholesterol in comparison to the “bad” cholesterol carrier, low-density lipoprotein, as it is believed to remove excess cholesterol from arterial

plaques. The major apolipoprotein component of HDL is apolipoprotein A-I (apoA-I), which is synthesized in the liver and intestine with a mature form composed of 243 residues.[1] To understand the functionality and physiological properties of apoA-I, a detailed knowledge of its tertiary structure is therefore required. The most studied apoA-I structure for a discoidal HDL is a "belt" structure: lipids are encircled by two antiparallel apoA-I proteins.[2-8] A "trefoil" model for a spherical HDL has also been proposed based on chemical cross-linking and mass spectrometry (CCL/MS) studies.[9] Due to the dynamic nature of apoA-I in solution, there is still no full-length lipid-free apoA-I structure available. However, several structural models of lipid-free apoA-I have been proposed based on CCL/MS results and molecular dynamics simulations.[10-13]

With the importance of HDL, numerous academic laboratories and the pharmaceutical industry have tried to develop HDL mimics for various therapeutic purposes.[14-15] Studies have demonstrated that functional mimics of HDL are able to bind and transport cholesterol.[16-18] Particularly, Thaxton and coworkers have employed a 5-6 nm diameter gold nanoparticle (AuNP) as a size and shape controllable scaffold to assemble 1,2-dipalmitoyl-sn-glycero-3-phosphocholine (DPPC), 1,2-dipalmitoyl-sn-glycero-3-phosphoethanolamine-N-[3-(2-pyridyldithio)propionate] (PDP PE), and apoA-I to form AuNP templated HDL-like nanoparticles (HDL AuNPs).[16] A follow-up study has demonstrated that this lipid-functionalized AuNP/protein construct is a robust passive and active acceptor of cellular cholesterol.[17] HDL AuNPs have shown potential as therapeutics for diseases of cholesterol overload, lymphoma, and other indications.[17, 19-22] AuNP conjugates are known to have high tailorability and biocompatibility, which makes them a natural candidate for such studies.[23] Moreover, AuNPs can be detected by their optical properties, so the lipid-functionalized AuNP is a promising agent

for monitoring critical human performance parameters of HDL, such as cholesterol transport, cellular cholesterol balance, and the inflammatory response.[24-25]

In order to further optimize the functionalized HDL AuNP for therapeutic use, it is essential to have detailed structural information about it. Experimental approaches such as high resolution transmission electron microscopy, X-ray photoelectron spectroscopy (XPS), and UV-vis spectroscopy have provided valuable insights into this aspect, yet detailed and localized structural information concerning the construct is still lacking.[26] Molecular dynamics (MD) simulation provides an alternative approach that may complement the current experimental limitations. In this study, we combined coarse-grained (CG) and all-atom (AA) MD simulations to simulate the self-assembly of lipids and cholesteryl ester on the AuNP/apoA-I construct to gain insights into its structural properties, and further make comparisons with XPS and functional results. Because the self-assembly of lipids on AuNP is likely to have a timescale longer than μs, it is not feasible to simulate this process directly using AA MD. Our general approach here is to simulate the lipid self-assembly process using the Martini CG model,[27-29] followed by switching the already assembled CG results to an AA model and performing AA simulations for structural analyses that can be compared with experiment.[30] We find strong agreement between theory and experiment, and our results provide detailed insight as to how the gold HDL-like nanoparticle construct can function similarly to native HDL in its uptake of cholesterol.

## RESULTS AND DISCUSSION

**Composition of HDL AuNP and simulation model.** Experiments have previously demonstrated that the HDL AuNP is composed of a 5-6 nm AuNP, a mixture of DPPC/PDP PE

lipids (~175:175), and ~3 apoA-I proteins.[16-17] It is suggested that the disulfide bond of the PDP PE lipid is broken during adsorption on the AuNP surface, resulting in thiolates of MPDP PE and 2-MPT (**Scheme S1**).[26] Because of the distinct interactions between the AuNP surface and these lipids, particularly due to the strong Au-S interaction (~50 kcal/mol), it is expected that the self-assembly of these two types of lipid on the AuNP will have different binding patterns. Directly simulating this HDL AuNP without understanding the pure lipid cases may lead to difficulty in interpreting the resulting morphology as there are many factors that can contribute to the final structure. Therefore, we started with a simple system consisting of only pure lipid (plus the Au particle), then a mixture of lipids, and finally the experimental HDL AuNP system. We placed a 5 nm AuNP in the center of a 210 Å x 210 Å x 210 Å cubic box and randomly placed the lipids inside this cubic box. A 5 μs CG simulation was performed to model the self-assembly process. After the lipids were well assembled on the AuNP surface, we backmapped the CG result to AA model and performed a 100 ns AA MD for structural analyses.

**Self-assembly of individual DPPC and MPDP-PE/2-MPT lipids on the AuNP.** We first attempted to simulate the self-assembly process at 300 K with 350 pure DPPC lipids. Unexpectedly, instead of binding to the AuNP, the DPPC lipids formed a bilayer membrane in the solution (**Figure S1**). It is possible that our 5 μs simulation time is not enough to sample the binding process. Another possibility is that the DPPC lipids are in a gel phase at 300 K that makes it less dynamic to diffuse to the AuNP surface. This can also be attributed to the rigid AuNP because this can make water molecules frozen around the solid surface. This has been a known limitation of Martini CG simulations.[27] To overcome this problem, we increased the simulation temperature. When the simulation temperature increased to 323 K, at which point the DPPC lipids are in a liquid phase, the DPPC lipids were able to self-assemble on the AuNP

within 5 μs. They wrapped around the AuNP and formed a donut-like structure with a diameter ~140 Å (**Figure 1A**). The lipid tails do not interdigitate in this structure, and the thickness of this bilayer is ~50 Å, which is the diameter of the AuNP. We also performed the same simulations with 240 or 160 DPPC lipids. Interestingly, a trefoil-like structure was found in the case of 240 DPPC lipids (**Figure 1B**). When the lipid number was reduced to 160, a donut-like conformation formed again, with a similar bilayer thickness but a smaller diameter of ~105 Å (**Figure S2**). In the donut-like structure, the DPPC lipids seemed to maintain a disc bilayer structure if we neglect the AuNP region (**Figure 1A**). As discoidal HDL forms a similar disc bilayer structure,[2] this suggests that AuNP can serve as a core replacement for discoidal HDL and the binding of the apoA-I on the AuNP HDL may have similar belt or trefoil structure. We did not intensively screen different numbers of DPPC lipids in this study since our primary interest was to understand systems involving lipid mixtures rather than the pure DPPC lipid system. As a result,

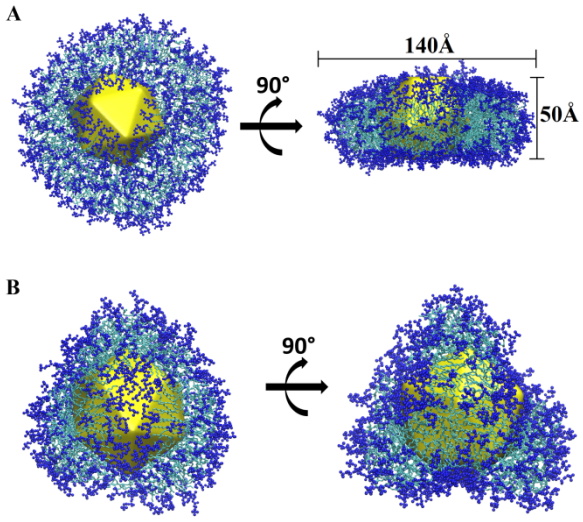


**Figure 1.** DPPC self-assembly on AuNP. (A) 350 DPPC lipids form a donut-like conformation. (B) 240 DPPC lipids form a trefoil conformation. AuNP is colored in yellow. Headgroups and tails are colored in blue and cyan, respectively.

we did not quantify the ranges in DPPC lipid numbers that lead to donut-like or trefoil-like structures. This and the equivalent studies of lipid mixtures may be interesting for further work.

For the MPDP PE/2-MPT lipids, because of the strong interaction between the sulfur group and gold, presumably they will self-assemble preferentially with sulfur coordinated to the AuNP surface. Indeed, in the case of 350 molecules of MPDP PE/2-MPT, all molecules were assembled on the AuNP within the 5 μs simulation time. The overall morphology was like a curved bilayer lipid membrane bound on the AuNP (**Figure 2A**). Most of the lipids in the inner layer were laid down on the AuNP surface and loosely packed (**Figure 2B**), while most of lipids in the outer layer were oriented perpendicularly to the AuNP surface (**Figure 2C**). The thicknesses of the inner and outer layers were ~17 Å and ~26 Å, respectively. As expected, the 2-MPT molecules are located mainly on the AuNP surface. In addition, no belt or trefoil

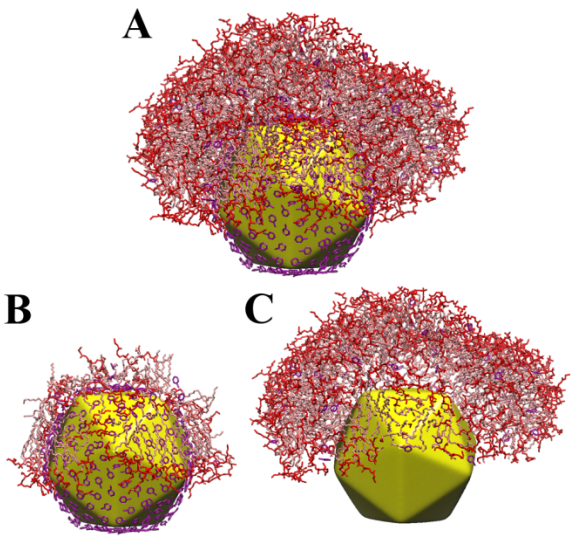


**Figure 2.** 350 MPDP PE/2-MPT lipids self-assembled on AuNP. (A) Overall morphology. (B) Inner layer. (C) Outer layer. Headgroup and tail regions are colored in red and pink, respectively. 2-MPT is colored in purple.

conformations were observed among different lipid numbers for MPDP PE/2-MPT. We also performed the same simulation with PDP PE lipid (instead of MPDP PE/2-MPT) and found similar layer thickness and morphologies (**Figure S3**).

**Self-assembly of a mixture of DPPC and MPDP-PE/2-MPT lipids on the AuNP.** Next, we simulated a mixture of DPPC/MPDP PE/2-MPT lipids (175:175:175) on the AuNP. In this mixed lipid case, the MPDP PE/2-MPT molecules seem to dominate the overall morphology. The two types of lipids mix together and form a bilayer structure on the AuNP surface with an overall morphology similar to the MPDP PE/2-MPT result described above (compare **Figures 3A and 2A**), suggesting the MPDP PE/2-MPT lipid dominates the overall bilayer structure in the DPPC/MPDP PE/2-MPT mixture lipids. This is attributed to the sulfur atoms of MPDP PE/2-MPT molecules that have stronger affinity to the AuNP surface. Moreover, because of the different binding strength of DPPC and MPDP PE/2-MPT on the AuNP surface, it is expected that their mixture will form an asymmetric bilayer structure on the AuNP with the inner layer having the higher propensity for the MPDP PE/2-MPT lipid. Indeed, a structural analysis showed that ~66 % MPDP-PE molecules were located in the inner layer, while ~65 % DPPC were in the outer layer. Within the same lipid layer, these two types of lipids were randomly distributed and did not have a clear clustering pattern (**Figures 3B and 3C**).

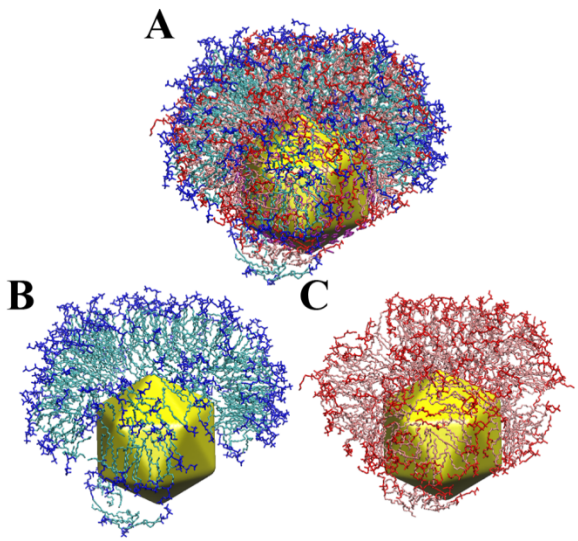


**Figure 3.** Self-assembly of mixture of DPPC/MPDP PE/2-MPT (175:175:175) on AuNP. The morphologies of lipids on AuNP with (A) all three lipids (B) DPPC lipid only and (C) MPDP PE lipid only. The same colors as in figures 1 and 2 are used.

**Self-assembly of DPPC/MPDP PE/2-MPT on two and three apoA-I loaded AuNP.** ApoA-I protein is known to have a well-defined amphipathic property, providing a domain boundary between lipids and solution that helps stabilize the overall structure of HDL. Experiment demonstrated that the HDL AuNP construct we studied contains ~3 apoA-I.[16] Given that the belt and trefoil structures of apoA-I on HDL have been proposed based on experiments,[2-9] and that the HDL AuNP is a mimic of HDL, we assumed that in the cases of two and three apoA-I in the HDL AuNP will form similar belt and trefoil structures on AuNP, respectively. We therefore preloaded the belt or trefoil apoA-I on the AuNP construct (**Figure S4**) and simulated the self-assembly of lipids on the AuNP.

We found that lipids are assembled differently on the regions with or without apoA-I protein. Figure 4A shows the overall morphology of the three apoA-I loaded case. The orientations of lipids have two distinct types. The first type is found in the region under apoA-I, where some lipid tails contact with apoA-I or the AuNP surface and the rest are packed in between them,

resulting in a horizontal orientation of lipids to the AuNP surface (**Figure 4B**). This type of orientation is similar to the case of pure DPPC lipids (**Figure 1A**). The second type is found in the region without apoA-I (**Figure 4C**), the orientation is similar to the mixture lipids case (**Figure 3**). In addition, the apoA-I proteins do not maintain a canonical trefoil structure. Instead, the trefoil conformation changes to a T-shape conformation, with a large sector and two small sectors. We find that the lipid orientations for the two apoA-I loaded results are similar to that for the three apoA-I loaded case (**Figure S5**). However, the two apoA-I loaded case have more of the perpendicular type of orientation since fewer apoA-I are in the HDL AuNP.

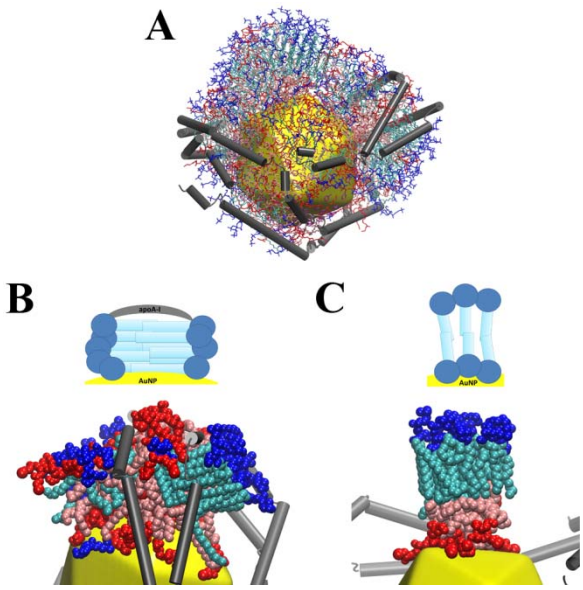


**Figure 4.** Self-assembly of a mixture of DPPC/MPDP PE/2-MPT (175:175:175) on three apoA-I loaded AuNPs. (A) Overall morphology. (B) Type I orientation. The lipids contact apoA-I with their tails and lay on the AuNP surface. (C) Type II orientation. The outer layer lipids orient perpendicularly to the AuNP surface, while the inner layer lipids mostly lay on the AuNP surface and pack loosely. The same colors as in figures 1 and 2 are used. ApoA-I is colored in gray.

**Distribution of lipids and apoA-I on the AuNP.** Previous qualitative XPS data suggested that the outer lipid layer of HDL AuNP is composed of mixture of PDP PE and DPPC bound to apoA-I.[26] However, the detailed composition of these lipids within outer or inner layers is not clear. In order to evaluate the distribution of lipids and apoA-I on the AuNP, we reanalyzed the XPS data and estimated that the outer lipid layer is composed of roughly 64-68 % DPPC lipid (see Supporting Information for details). In order to make comparison to the XPS data, we calculated the radial distribution function (RDF) of specific molecules in the HDL AuNP.

As mentioned earlier, the molecules that contain sulfur, 2-MPT and MPDP PE, prefer to stay on the AuNP surface. Indeed, we found that 2-MPT has a sharp peak at ~28 Å, which is in the AuNP surface region (**Figures 5 and S6**). For the MPDP PE lipids, the peak is at ~33 Å, which also indicates that this lipid prefers binding to the AuNP surface. Since DPPC lipids have weaker interaction with the AuNP, it is not surprising that the majority of them are not located on the AuNP surface. By taking a 42 Å cutoff (as the inner layer is ~17 Å thick) to separate inner and outer lipid layers for the above RDFs, the outer layer is composed of 67 % and 64 % DPPC in the two and three apoA-I loaded AuNP systems, respectively. In addition to the above RDF,

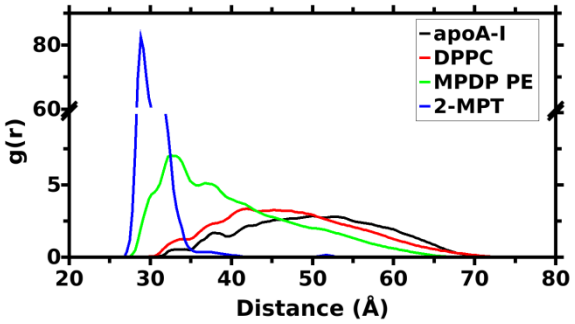


**Figure 5.** Radial distribution function (RDF) of DPPC/MPDP PE/2-MPT (175:175:175) on three apoA-I loaded HDL AuNP.

which was calculated based on whole molecules, we also calculated RDFs for the nitrogen atoms of DPPC and MPDP PE (**Figure S7**), which provides a more quantitative comparison to the experimental XPS data. **Table 1** shows that the whole molecule and nitrogen atom RDFs are very similar. It is worth noting that it is possible that the extraction step of the outer layer lipid in experiment peels only outer layer lipids from the non-apoA-I region. In other words, lipids in the space between the AuNP surface and apoA-I are protected by apoA-I and may not be successfully extracted. In that case, a larger discrepancy between the simulation and experiment may arise, especially in high apoA-I loaded AuNP.

**Table 1.** Percentage of DPPC in the outer layer.

| | Cholesteryl ester | DPPC (%)[a] | DPPC (%)[b] |
|---|---|---|---|
| **Two apoA-I** | 0 | 64 | 67 |
| | 20 | 67 | 68 |
| | 100 | 58 | 63 |
| **Three apoA-I** | 0 | 67 | 74 |
| | 20 | 63 | 67 |
| | 100 | 55 | 60 |

[a]calculated from whole molecule RDFs.

[b]calculated from N atom RDFs.

A 42 Å cutoff in RDFs was used to separate inner and outer layer.

**Distribution of cholesteryl ester on the functionalized HDL AuNP.** Given that our simulation results are in line with the experimental lipid distribution for the AuNP construct, we next considered the distribution of cholesteryl ester on the construct using MD simulations. To address this question, we simulated with 20 or 100 cholesteryl esters, which account for ~1 % or

5 % volume of AuNP HDL, respectively. We simulated each condition with either two and three apoA-I using the same CG and AA simulations, mixing cholesteryl ester molecules with DPPC/MPDP PE/2-MPT (175:175:175) lipids from the beginning of the simulations.

The RDFs from constructs that consist of either two or three apoA-I loaded with lipids and 20 cholesteryl ester molecules on a AuNP revealed that the cholesteryl ester molecules were distributed mainly near the AuNP surface, which was near the core region of the HDL mimic (**Figures 6 and S8**). For the rest of the molecules in the construct, their distributions were very similar to what we found without cholesteryl ester. When 100 cholesteryl ester molecules were loaded onto the HDL AuNP, they were still mainly found near the core region of the AuNP construct, however, with a less sharp peak in the RDF compared to when only 20 molecules were included (**Figures S9 and S10)**. Past experimental work has suggested that the inner core of a native HDL has a higher concentration of cholesteryl ester and that the packing of cholesteryl ester in the particle core maintains a reverse concentration gradient that can assist in binding

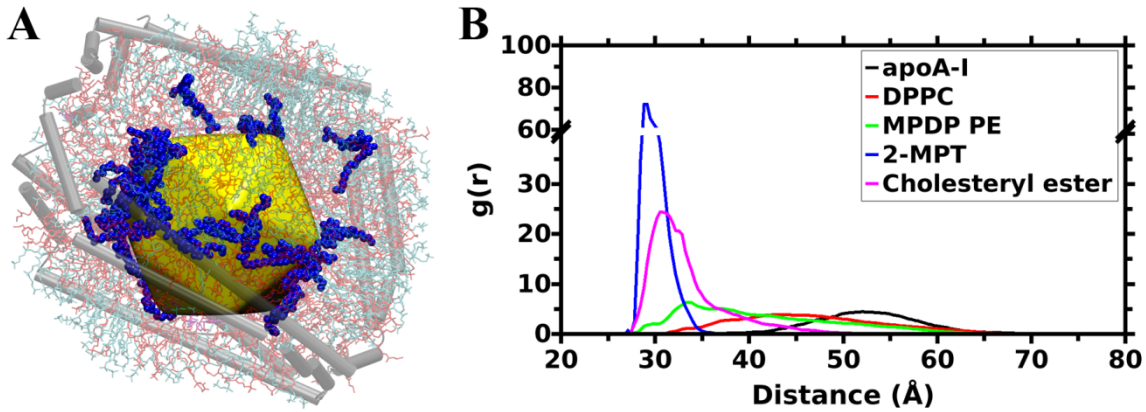


**Figure 6.** Self-assembly of a mixture of DPPC/MPDP PE/2-MPT/cholesteryl ester (175:175:175:20) on three apoA-I loaded AuNPs. (A) Overall structure. (B) RDF. Cholesteryl ester is colored in blue.

more free cholesterol to the surface of HDL.[31] Our findings on cholesteryl ester binding and moving close to the gold nanoparticle is encouraging and suggests that the functionalized HDL AuNP can bind cholesterol in a somewhat similar manner to native HDL.

**Measurement of cholesterol and cholesteryl ester in HDL AuNPs incubated with LCAT**. Lecithin:cholesterol acyltransferase (LCAT) is known to bind HDL particles, is activated by apoA-I, and converts free cholesterol to cholesteryl ester that is then sequestered in the core of HDL. As modeling data show that HDL AuNPs support cholesteryl ester binding to the core region of the particle, we directly measured if the HDL AuNP can activate LCAT and support binding of cholesteryl ester. First, we added free cholesterol to a solution of HDL AuNPs. Next, we added purified human LCAT into solution and incubated the mixture overnight. Using the Amplex Red assay, we were able to quantify the amount of cholesterol and cholesteryl ester on the HDL AuNPs. By conducting the assay with and without cholesterol esterase, it is possible to determine the contribution of cholesteryl esters to the total measured amount of cholesterol on the HDL AuNPs. Using this method, we determined that the HDL AuNPs have both free and esterified cholesterol after incubation with LCAT (**Figure 7A**). Further, these data indicate that cholesteryl ester makes up ~16 % of the total cholesterol bound to the HDL AuNP. As a control, HDL AuNP without apoA-I (Bilayer NP) incubated with cholesterol and LCAT did not support cholesteryl ester formation (**Figure 7B**), demonstrating the requirement for apoA-I as an activator of LCAT and the formation of cholesteryl ester. The modeling data support that the esterified cholesterol can assume a more central location within the HDL AuNP particle.

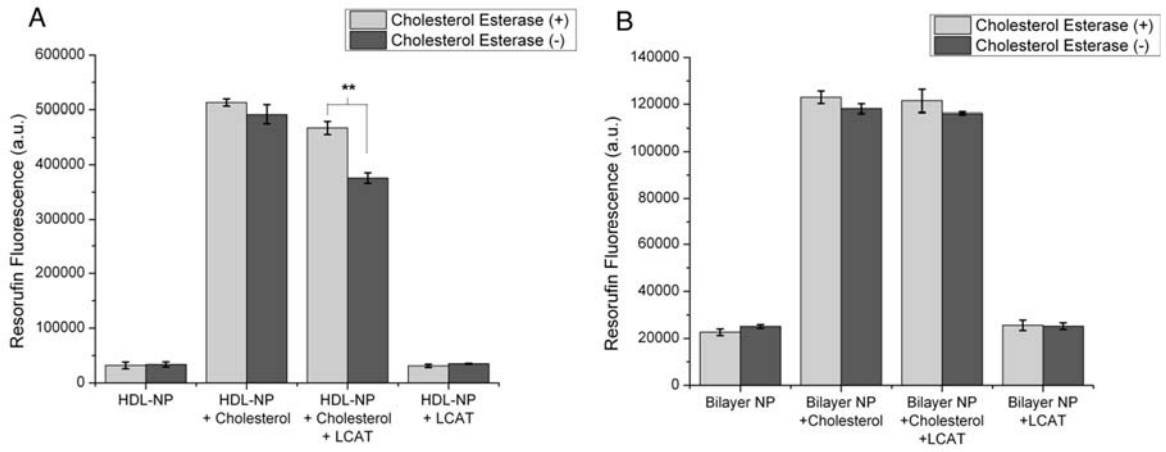


**Figure 7.** HDL AuNP support the activation of LCAT, as measured through Amplex Red based fluorescence measurement of cholesterol and cholesteryl ester. (A) In the presence of cholesterol and LCAT, a significant amount of cholesteryl ester is detected (**$p<0.005$, N=3 per group). (B) No significant amount of cholesteryl ester was detected using HDL AuNP without apoAI (Bilayer NP) in the presence of cholesterol and LCAT, confirming the specific activity of LCAT on HDL AuNPs that contain apoA-I.

**Simulation limitations and future perspective.** In this study we have assumed that the apoA-I forms either a belt or trefoil structure on the AuNP as these two structures are the most commonly studied models. However, we cannot exclude the possibility that other apoA-I structures occur, such as double superhelix,[32] helix-dimer hairpin,[33] or horseshoe structures,[34] and it is not possible with our current simulation technology to determine which one is correct. Future studies that combine both theory and experiment will be required to further address this question. Another limitation is that since the gold-sulfur portion of the force field is a simple two-body potential, it might not be able to fully describe the influence of facets, edges and points on the icosahedral gold particle. In addition, as human HDL contains different compositions of

phospholipid, the study of different combinations and types of lipids will be important in providing critical information in diagnostic and therapeutic applications involving HDL AuNP.

## CONCLUSION

In this study, we have demonstrated the potential of computer simulation in modeling a previously designed AuNP-functionalized HDL construct by using CG and AA MD simulations. Based on our work, and as a starting point, we found that loading 160 and 350 pure DPPC lipids on the 5 nm AuNP surface led to a donut-like conformation, while a trefoil-like conformation was found in the case of 240 DPPC lipids. This result provides comparison to natural HDLs where the apoA-I is found to associate in discoidal and spherical HDLs in similar fashion; however, this system is not as directly comparable with the HDL AuNPs. More directly, when DPPC/MPDP PE/2-MPT (175:175:175) were loaded on the AuNP with two or three apoA-I proteins, the lipids had distinct orientations in the regions with or without apoA-I. In the region with apoA-I, the lipids orient horizontally to the AuNP surface, while in the region without apoA-I the outer layer lipids orient perpendicularly to the AuNP surface and the inner layer lipids pack loosely or lay on the AuNP. RDF analyses demonstrate that molecules containing sulfur, such as 2-MPT and MPDP PE, were mainly located on the AuNP surface. In addition, the outer layer lipids were composed of 64-74 % of DPPC, which is in close correspondence with experimental results based on quantitative XPS measurements. Collectively, these data correspond with published functional data demonstrating that the HDL AuNP supports cholesterol efflux from cells by way of a receptor typically accessed by lipid-poor apoA-I, namely ATP-binding cassette transporter A-1 (ABCA1), and also through receptors more associated with binding lipid rich apoA-I associated with more cholesterol-rich HDLs, like

ABCG1 and scavenger receptor type B-1. Finally, we showed that cholesteryl ester molecules are mostly in close proximity to the AuNP surface somewhat analogous to the core region of native HDL. The cholesteryl ester distribution and functional data suggest that the HDL AuNP construct is able to maintain a surface-to-core (low to high) concentration gradient similar to the gradient in native HDL. Incubating the HDL AuNP with cholesterol and LCAT demonstrate the HDL AuNP is able to efficiently activate LCAT and form esterified cholesterol from free cholesterol and phospholipid.

Our findings have demonstrated the value and great potential of computational approaches from an atomistic model in bridging the knowledge gap between experimental observations and particularly in this case, helping us to better describe the functionalized HDL AuNP. While we only considered belt and trefoil loaded apoA-I structures in this study, the resulting simulation protocols can be applied to other apoA-I models as well as to different lipid types. Further study of different lipid mixtures as well as different apoA-I models will be interesting and valuable to the HDL AuNP field.

## METHODS

**Coarse-grained MD simulation.** Based on the most recent experimental results, the shape of the 5 nm AuNP used in the experiments is icosahedral rather than spherical as previously assumed.[26] Moreover, the disulfide bond of the PDP PE lipid is broken during adsorption, resulting in thiolates of 1,2-dipalmitoyl-sn-glycero-3-phosphoethanolamine-N-3-mercaptopropionate (denoted as MPDP PE) and 2-mercaptopyridine (denoted as 2-MPT) (**Scheme S1**). Therefore, MPDP PE and 2-MPT molecules were used in the simulation instead of the PDP PE lipid. The Martini v2.2 CG model and force fields were used.[27-28] MPDP PE and 2-

MPT force fields were parameterized using the auto-martini tools[35] with adjustments to match the all atom MD results. Details of the force fields are listed in the Supporting Information. The gold force field was taken from another study.[36] A 5 nm icosahedral AuNP was built using a script from OpenMD[37] software. For those studies having apoA-I present, a belt or trefoil structure of lipoprotein apoA-I was placed on the AuNP to define initial structures for the simulations. Lipids were randomly placed in a 210 Å x 210 Å x 210 Å cubic box using the packmol package.[38] Each system was solvated with ~7000 CG water molecules. 10% of the water molecules were replaced with anti-freeze water molecules. $Na^+$ ions were added to neutralize the net charge of the system. All CG MD simulations were carried out using GROMACS 4.5.6[39] with standard simulation parameters associated with the Martini force field. Simulations were performed under the NPT ensemble. Unless specifically mentioned, the simulation temperature was 300 K. A 5 μs production run was performed for each case. For the apoA-I loaded cases, to prevent the apoA-I from collapsing on the AuNP before lipid self-assembly on the AuNP, we restrained the apoA-I structure and let the lipids be free to self-assemble on the AuNP first. This was done by applying 500 kJ/mol Cartesian restraints to the protein during the first 1 μs. The rest of the production run was unrestrained except for the gold atoms which were always fixed. We performed two independent runs for both the 2 and 3 apoA-I loaded DPPC/MPDP PE/2-MPT/cholesteryl ester (175:175:175:100) systems, the most complicated systems in our study, and found that overall morphologies from the two independent runs are similar (**Figure S11**). Therefore, we only performed one run for the remaining cases.

**All-atom MD simulation.** The initial structures for all-atom simulations were extracted from the last snapshot of the 5 μs CG results. The backward mapping procedure (CG to AA) is adapted from other studies.[30] Each system was neutralized with $Na^+$ ions and solvated in a

truncated octahedral box with ~56000 TIP3P water molecules. AMBER ff14SB,[40] lipid14,[41] and GAFF[42] force fields were used. The gold force field was adapted from earlier work.[43] AA MD simulations were carried out using AMBER 14.[44] SHAKE was used to constrain bonds to hydrogen.[45] The particle mesh Ewald method was used for calculating electrostatic energy with a 10Å nonbonded cutoff. Each system was equilibrated as follows. First, the system was minimized for 5000 steps, and subsequently heated from 100 to 300 K in 500 ps under constant volume condition. During the heating process, 10 kcal/mol/$A^2$ Cartesian restraints were applied to the proteins and lipids. Next, the system was switched to a NPT ensemble at 1 atm and 300 K for 500 ps with the same restraints. Then, a 500 ps run with 1 kcal/mol/$A^2$ restraints was performed. After the system was equilibrated, a 100 ns unrestraint production run was performed for each system under the NPT condition of 1 atm and 300 K. Gold atoms were restrained during the whole simulation. To test the convergence, we measured the RMSD of the apoA-I structure from the 3 apoA-I loaded DPPC/MPDP PE/2-MPT/cholesteryl ester (175:175:175:100) system and found that protein structure is relatively stable after 50 ns (**Figure S12**). Therefore, the last 50 ns results were taken for structural analyses.

**Experimental characterization of HDL AuNP.** The XPS measurements were performed as described in an earlier paper.[26] A detailed analysis of intensity results was performed to determine the relative populations of the various components. Results of this analysis are given in the Supporting Information.

**Measurement of Cholesteryl Ester Formation on HDL AuNP.** The HDL AuNP and Bilayer NP (HDL AuNP without apoA-I) were synthesized as previously described.[17] After synthesis, HDL AuNPs and Bilayer NPs were loaded with cholesterol by adding 10 µl of a 1 mg/ml stock solution of cholesterol in ethanol to 250 µl of 100 nM NPs. For LCAT-treated groups, 10 µl of a

10 nM stock solution of LCAT was added to 250 µl of NPs and allowed to incubate overnight at 37°C. Following overnight incubation of NPs with cholesterol and LCAT, the NPs were purified by centrifugation. Free cholesterol was measured using an Amplex Red Cholesterol Assay Kit (Thermo Fisher Scientific, Waltham, MA), as per the instructions provided by the manufacturer. For cholesteryl ester measurements, cholesterol esterase was omitted from the test reagents. A students *t*-test was utilized to analyze data, with $p<0.05$ demonstrating statistical significance.

## ASSOCIATED CONTENT

**Supporting Information**. Complete XPS analysis, additional figures, and force fields. This material is available free of charge via the Internet at http://pubs.acs.org.

## AUTHOR INFORMATION

### Corresponding Author

*(G.C.S.) E-mail g-schatz@northwestern.edu.

### Author Contributions

The manuscript was written through contributions of all authors. All authors have given approval to the final version of the manuscript.

### Notes

The authors declare no competing financial interest.

## ACKNOWLEDGMENT

This material is based on research sponsored by the Air Force Research Laboratory under agreement number FA8650-15-2-5518. The U.S. Government is authorized to reproduce and distribute reprints for Governmental purposes notwithstanding any copyright notation thereon. The views and conclusions contained herein are those of the authors and should not be interpreted as necessarily representing the official policies or endorsements, either expressed or implied, of Air Force Research Laboratory or the U.S. Government. We also thank NSF Grant CHE-1465045. Computations were done on the Carbon cluster of the Center for Nanoscale Materials at Argonne National Laboratory. Use of the Center for Nanoscale Materials, an Office of Science user facility, was supported by the U. S. Department of Energy, Office of Science, Office of Basic Energy Sciences, under Contract No. DE-AC02-06CH11357.

## ABBREVIATIONS

2-MPT, 2-mercaptopyridine thiolate; all-atom, AA; apoA-I, apolipoprotein A-I; AuNP, gold nanoparticle; CG, coarse-grained; DPPC, 1,2-dipalmitoyl-sn-glycero-3-phosphocholine; HDL, high density lipoprotein; LCAT, lecithin–cholesterol acyltransferase; MD, molecular dynamics; MPDP PE, 1,2-dipalmitoyl-sn-glycero-3-phosphoethanolamine-N-3-mercaptopropionate; PDP PE, 1,2-dipalmitoyl-sn-glycero-3-phosphoethanolamine-N-[3-(2-pyridyldithio)propionate]; RMSD, root-mean-square deviation; XPS, X-ray photoelectron spectroscopy.

## REFERENCES

1. Nofer, J. R.; Kehrel, B.; Fobker, M.; Levkau, B.; Assmann, G.; von Eckardstein, A., HDL and Arteriosclerosis: Beyond Reverse Cholesterol Transport. *Atherosclerosis* **2002,** *161* (1), 1-16.

2. Borhani, D. W.; Rogers, D. P.; Engler, J. A.; Brouillette, C. G., Crystal Structure of Truncated Human Apolipoprotein A-I Suggests a Lipid-bound Conformation. *Proceedings of the National Academy of Sciences* **1997,** *94* (23), 12291-12296.

3. Segrest, J. P.; Jones, M. K.; Klon, A. E.; Sheldahl, C. J.; Hellinger, M.; De Loof, H.; Harvey, S. C., A Detailed Molecular Belt Model for Apolipoprotein A-I in Discoidal High Density Lipoprotein. *Journal of Biological Chemistry* **1999,** *274* (45), 31755-31758.
4. Tricerri, M. A.; Behling Agree, A. K.; Sanchez, S. A.; Jonas, A., Characterization of Apolipoprotein A-I Structure Using a Cysteine-Specific Fluorescence Probe. *Biochemistry* **2000,** *39* (47), 14682-14691.
5. Davidson, W. S.; Hilliard, G. M., The Spatial Organization of Apolipoprotein A-I on the Edge of Discoidal High Density Lipoprotein Particles: A MASS SPECTROMETRY STUDY. *Journal of Biological Chemistry* **2003,** *278* (29), 27199-27207.
6. Martin, D. D. O.; Budamagunta, M. S.; Ryan, R. O.; Voss, J. C.; Oda, M. N., Apolipoprotein A-I Assumes a "Looped Belt" Conformation on Reconstituted High Density Lipoprotein. *Journal of Biological Chemistry* **2006,** *281* (29), 20418-20426.
7. Bhat, S.; Sorci-Thomas, M. G.; Tuladhar, R.; Samuel, M. P.; Thomas, M. J., Conformational Adaptation of Apolipoprotein A-I to Discretely Sized Phospholipid Complexes. *Biochemistry* **2007,** *46* (26), 7811-7821.
8. Wu, Z.; Wagner, M. A.; Zheng, L.; Parks, J. S.; Shy, J. M.; Smith, J. D.; Gogonea, V.; Hazen, S. L., The Refined Structure of Nascent HDL Reveals a Key Functional Domain for Particle Maturation and Dysfunction. *Nat Struct Mol Biol* **2007,** *14* (9), 861-868.
9. Huang, R.; Silva, R. A. G. D.; Jerome, W. G.; Kontush, A.; Chapman, M. J.; Curtiss, L. K.; Hodges, T. J.; Davidson, W. S., Apolipoprotein A-I Structural Organization in High-density Lipoproteins Isolated from Human Plasma. *Nat Struct Mol Biol* **2011,** *18* (4), 416-422.
10. Silva, R. A. G. D.; Hilliard, G. M.; Fang, J.; Macha, S.; Davidson, W. S., A Three-Dimensional Molecular Model of Lipid-Free Apolipoprotein A-I Determined by Cross-Linking/Mass Spectrometry and Sequence Threading. *Biochemistry* **2005,** *44* (8), 2759-2769.
11. Pollard, R. D.; Fulp, B.; Samuel, M. P.; Sorci-Thomas, M. G.; Thomas, M. J., The Conformation of Lipid-Free Human Apolipoprotein A-I in Solution. *Biochemistry* **2013,** *52* (52), 9470-9481.
12. Segrest, J. P.; Jones, M. K.; Shao, B.; Heinecke, J. W., An Experimentally Robust Model of Monomeric Apolipoprotein A-I Created from a Chimera of Two X-ray Structures and Molecular Dynamics Simulations. *Biochemistry* **2014,** *53* (48), 7625-7640.
13. Zhang, X.; Lei, D.; Zhang, L.; Rames, M.; Zhang, S., A Model of Lipid-Free Apolipoprotein A-I Revealed by Iterative Molecular Dynamics Simulation. *PLoS ONE* **2015,** *10* (3), e0120233.
14. Kingwell, B. A.; Chapman, M. J.; Kontush, A.; Miller, N. E., HDL-targeted Therapies: Progress, Failures and Future. *Nat Rev Drug Discov* **2014,** *13* (6), 445-464.
15. Lacko, A. G.; Sabnis, N. A.; Nagarajan, B.; McConathy, W. J., HDL as a Drug and Nucleic Acid Delivery Vehicle. *Front Pharmacol* **2015,** *6*, 247.
16. Thaxton, C. S.; Daniel, W. L.; Giljohann, D. A.; Thomas, A. D.; Mirkin, C. A., Templated Spherical High Density Lipoprotein Nanoparticles. *Journal of the American Chemical Society* **2009,** *131* (4), 1384-1385.
17. Luthi, A. J.; Lyssenko, N. N.; Quach, D.; McMahon, K. M.; Millar, J. S.; Vickers, K. C.; Rader, D. J.; Phillips, M. C.; Mirkin, C. A.; Thaxton, C. S., Robust Passive and Active Efflux of Cellular Cholesterol to a Designer Functional Mimic of High Density Lipoprotein. *Journal of Lipid Research* **2015,** *56* (5), 972-985.
18. Zhao, Y.; Imura, T.; Leman, L. J.; Curtiss, L. K.; Maryanoff, B. E.; Ghadiri, M. R., Mimicry of High-Density Lipoprotein: Functional Peptide–Lipid Nanoparticles Based on

Multivalent Peptide Constructs. *Journal of the American Chemical Society* **2013,** *135* (36), 13414-13424.

19. Yang, S.; Damiano, M. G.; Zhang, H.; Tripathy, S.; Luthi, A. J.; Rink, J. S.; Ugolkov, A. V.; T. K. Singh, A.; Dave, S. S.; Gordon, L. I.; Thaxton, C. S., Biomimetic, Synthetic HDL Nanostructures for Lymphoma. *Proceedings of the National Academy of Sciences* **2013,** *110* (7), 2511-2516.

20. Plebanek, M. P.; Mutharasan, R. K.; Volpert, O.; Matov, A.; Gatlin, J. C.; Thaxton, C. S., Nanoparticle Targeting and Cholesterol Flux Through Scavenger Receptor Type B-1 Inhibits Cellular Exosome Uptake. *Scientific Reports* **2015,** *5*, 15724.

21. Angeloni, N. L.; McMahon, K. M.; Swaminathan, S.; Plebanek, M. P.; Osman, I.; Volpert, O. V.; Thaxton, C. S., Pathways for Modulating Exosome Lipids Identified By High-Density Lipoprotein-Like Nanoparticle Binding to Scavenger Receptor Type B-1. *Scientific Reports* **2016,** *6*, 22915.

22. McMahon, K. M.; Mutharasan, R. K.; Tripathy, S.; Veliceasa, D.; Bobeica, M.; Shumaker, D. K.; Luthi, A. J.; Helfand, B. T.; Ardehali, H.; Mirkin, C. A.; Volpert, O.; Thaxton, C. S., Biomimetic High Density Lipoprotein Nanoparticles For Nucleic Acid Delivery. *Nano Letters* **2011,** *11* (3), 1208-1214.

23. Huang, X.; Jain, P. K.; El-Sayed, I. H.; El-Sayed, M. A., Gold Nanoparticles: Interesting Optical Properties and Recent Applications in Cancer Diagnostics and Therapy. *Nanomedicine* **2007,** *2* (5), 681-693.

24. Khera, A. V.; Cuchel, M.; de la Llera-Moya, M.; Rodrigues, A.; Burke, M. F.; Jafri, K.; French, B. C.; Phillips, J. A.; Mucksavage, M. L.; Wilensky, R. L.; Mohler, E. R.; Rothblat, G. H.; Rader, D. J., Cholesterol Efflux Capacity, High-Density Lipoprotein Function, and Atherosclerosis. *New England Journal of Medicine* **2011,** *364* (2), 127-135.

25. Welty, F., How Do Elevated Triglycerides and Low HDL-Cholesterol Affect Inflammation and Atherothrombosis? *Curr Cardiol Rep* **2013,** *15* (9), 1-13.

26. Sun, W.; Wu, W.; McMahon, K. M.; Rink, J. S.; Thaxton, C. S., Mosaic Interdigitated Structure in Nanoparticle-Templated Phospholipid Bilayer Supports Partial Lipidation of Apolipoprotein A-I. *Particle & Particle Systems Characterization* **2016,** *33* (6), 300-305.

27. Marrink, S. J.; Risselada, H. J.; Yefimov, S.; Tieleman, D. P.; de Vries, A. H., The MARTINI Force Field: Coarse Grained Model for Biomolecular Simulations. *J Phys Chem B* **2007,** *111* (27), 7812-24.

28. de Jong, D. H.; Singh, G.; Bennett, W. F. D.; Arnarez, C.; Wassenaar, T. A.; Schäfer, L. V.; Periole, X.; Tieleman, D. P.; Marrink, S. J., Improved Parameters for the Martini Coarse-Grained Protein Force Field. *Journal of Chemical Theory and Computation* **2013,** *9* (1), 687-697.

29. Ingólfsson, H. I.; Lopez, C. A.; Uusitalo, J. J.; de Jong, D. H.; Gopal, S. M.; Periole, X.; Marrink, S. J., The Power of Coarse Graining in Biomolecular Simulations. *Wiley Interdisciplinary Reviews: Computational Molecular Science* **2014,** *4* (3), 225-248.

30. Wassenaar, T. A.; Pluhackova, K.; Böckmann, R. A.; Marrink, S. J.; Tieleman, D. P., Going Backward: A Flexible Geometric Approach to Reverse Transformation from Coarse Grained to Atomistic Models. *Journal of Chemical Theory and Computation* **2014,** *10* (2), 676-690.

31. Illiana, M.; Miranda Van, E.; Theo, J. C. V. B., High-Density Lipoprotein: Key Molecule in Cholesterol Efflux and the Prevention of Atherosclerosis. *Current Pharmaceutical Design* **2010,** *16* (13), 1445-1467.

32. Wu, Z.; Gogonea, V.; Lee, X.; Wagner, M. A.; Li, X.-M.; Huang, Y.; Undurti, A.; May, R. P.; Haertlein, M.; Moulin, M.; Gutsche, I.; Zaccai, G.; DiDonato, J. A.; Hazen, S. L., Double Superhelix Model of High Density Lipoprotein. *Journal of Biological Chemistry* **2009,** *284* (52), 36605-36619.

33. Wu, Z.; Gogonea, V.; Lee, X.; May, R. P.; Pipich, V.; Wagner, M. A.; Undurti, A.; Tallant, T. C.; Baleanu-Gogonea, C.; Charlton, F.; Ioffe, A.; DiDonato, J. A.; Rye, K.-A.; Hazen, S. L., The Low Resolution Structure of ApoA1 in Spherical High Density Lipoprotein Revealed by Small Angle Neutron Scattering. *Journal of Biological Chemistry* **2011,** *286* (14), 12495-12508.

34. Gogonea, V.; Gerstenecker, G. S.; Wu, Z.; Lee, X.; Topbas, C.; Wagner, M. A.; Tallant, T. C.; Smith, J. D.; Callow, P.; Pipich, V.; Malet, H.; Schoehn, G.; DiDonato, J. A.; Hazen, S. L., The Low-resolution Structure of nHDL Reconstituted with DMPC with and without Cholesterol Reveals a Mechanism for Particle Expansion. *J Lipid Res* **2013,** *54* (4), 966-83.

35. Bereau, T.; Kremer, K., Automated Parametrization of the Coarse-Grained Martini Force Field for Small Organic Molecules. *Journal of Chemical Theory and Computation* **2015,** *11* (6), 2783-2791.

36. Lin, J.; Zhang, H.; Chen, Z.; Zheng, Y., Penetration of Lipid Membranes by Gold Nanoparticles: Insights into Cellular Uptake, Cytotoxicity, and Their Relationship. *ACS Nano* **2010,** *4* (9), 5421-5429.

37. Gezelter, J.; Kuang, S.; Marr, J.; Stocker, K.; Li, C.; Vardeman, C.; Lin, T.; Fennell, C.; Sun, X.; Daily, K., OpenMD, an Open Source Engine for Molecular Dynamics. University of Notre Dame: Notre Dame, IN: **2010**.

38. Martínez, L.; Andrade, R.; Birgin, E. G.; Martínez, J. M., PACKMOL: A Package for Building Initial Configurations for Molecular Dynamics Simulations. *Journal of Computational Chemistry* **2009,** *30* (13), 2157-2164.

39. Pronk, S.; Pall, S.; Schulz, R.; Larsson, P.; Bjelkmar, P.; Apostolov, R.; Shirts, M. R.; Smith, J. C.; Kasson, P. M.; van der Spoel, D.; Hess, B.; Lindahl, E., GROMACS 4.5: a High-throughput and Highly Parallel Open Source Molecular Simulation Toolkit. *Bioinformatics* **2013,** *29* (7), 845-54.

40. Maier, J. A.; Martinez, C.; Kasavajhala, K.; Wickstrom, L.; Hauser, K. E.; Simmerling, C., ff14SB: Improving the Accuracy of Protein Side Chain and Backbone Parameters from ff99SB. *Journal of Chemical Theory and Computation* **2015,** *11* (8), 3696-3713.

41. Dickson, C. J.; Madej, B. D.; Skjevik, A. A.; Betz, R. M.; Teigen, K.; Gould, I. R.; Walker, R. C., Lipid14: The Amber Lipid Force Field. *J Chem Theory Comput* **2014,** *10* (2), 865-879.

42. Wang, J.; Wolf, R. M.; Caldwell, J. W.; Kollman, P. A.; Case, D. A., Development and Testing of a General Amber Force Field. *J Comput Chem* **2004,** *25* (9), 1157-74.

43. Heinz, H.; Vaia, R. A.; Farmer, B. L.; Naik, R. R., Accurate Simulation of Surfaces and Interfaces of Face-Centered Cubic Metals Using 12−6 and 9−6 Lennard-Jones Potentials. *The Journal of Physical Chemistry C* **2008,** *112* (44), 17281-17290.

44. Case, D.; Babin, V.; Berryman, J.; Betz, R.; Cai, Q.; Cerutti, D.; Cheatham III, T.; Darden, T.; Duke, R.; Gohlke, H.; Goetz, A.; Gusarov, S.; Homeyer, N.; Janowski, P.; Kaus, J.; Kolossváry, I.; Kovalenko, A.; Lee, T.-S.; LeGrand, S.; Luchko, T.; Luo, R.; Madej, B.; Merz, K.; Paesani, F.; Roe, D.; Roitberg, A.; Sagui, C.; Salomon-Ferrer, R.; Seabra, G.; Simmerling, C.; Smith, W.; Swails, J.; Walker, R.; Wang, J.; Wolf, R.; Wu, X.; Kollman, P. *Amber 14*, University of California, San Francisco: **2014**.

45. Ryckaert, J.-P.; Ciccotti, G.; Berendsen, H. J. C., Numerical Integration of the Cartesian Equations of Motion of a System with Constraints: Molecular Dynamics of n-alkanes. *Journal of Computational Physics* **1977,** *23* (3), 327-341.

TOC